

This is the accepted manuscript made available via CHORUS. The article has been published as:

## Measurement of the Adiabatic Index in Be Compressed by Counterpropagating Shocks

C. Fortmann, H. J. Lee, T. Döppner, R. W. Falcone, A. L. Kritcher, O. L. Landen, and S. H. Glenzer

Phys. Rev. Lett. **108**, 175006 — Published 25 April 2012

DOI: [10.1103/PhysRevLett.108.175006](https://doi.org/10.1103/PhysRevLett.108.175006)

# Measurement of the adiabatic index in Be compressed by counter-propagating shocks

C. Fortmann,<sup>1,2</sup> H. J. Lee,<sup>3</sup> T. Döppner,<sup>1</sup> R. W. Falcone,<sup>4</sup> A. L. Kritcher,<sup>1</sup> O. L. Landen,<sup>1</sup> and S. H. Glenzer<sup>1</sup>

<sup>1</sup>*Lawrence Livermore National Laboratory, Livermore, CA 94551, USA*

<sup>2</sup>*Department of Physics and Astronomy, University of California, Los Angeles, CA 90095, USA*

<sup>3</sup>*SLAC National Accelerator Laboratory, 2575 Sand Hill Rd. Menlo Park, CA 94025*

<sup>4</sup>*Department of Physics, University of California, Berkeley, CA 94720, USA*

We report on the first direct measurement of the adiabatic index  $\gamma$  through X-ray Thomson Scattering from shock-compressed beryllium. 9 keV x-ray photons probe the bulk properties of matter during the collision of two counter-propagating shocks. This novel experimental technique determines  $\gamma$  using only the measured mass densities and vanishing particle velocity at the point of shock collision to close the Rankine-Hugoniot equations. We find  $\gamma > 5/3$  at 3x compression, clearly different from ideal gas behavior. At 6x compression,  $\gamma$  shows the convergence to the ideal gas limit, in agreement with linear scaling laws.

PACS numbers: 52.25.Os, 61.05.cf, 78.70.Ck, 52.50.Lp

Compression of solid targets by intense laser radiation generates superdense matter with many times solid density, temperatures of several 10000 K, and pressures in excess of 1 Mbar. These extreme states of matter serve as model systems to investigate astrophysical objects that exist at similar conditions. Studying the Equation of State (EoS) of matter at extreme conditions is vital for inertial confinement fusion [1] experiments, where matter is compressed up to 1000 g/cm<sup>3</sup>. The adiabatic index, i.e. the shock gamma  $\gamma = 1 + p/\rho\varepsilon$ , with pressure  $p$ , mass density  $\rho$  and energy density  $\varepsilon$  [2], is a central quantity. For perfect gases,  $\gamma$  is the ratio of heat capacities at constant pressure and volume  $c_p/c_v$ , respectively and can also be expressed through the sound speed  $\gamma = \gamma_S = c_s^2\rho/p$ . In non-ideal dense plasmas, the shock gamma, sound speed gamma and the heat capacities become density dependent and are no longer equal.

Beryllium is a candidate capsule ablator material in inertial confinement fusion (ICF) experiments [3]. Knowledge of its thermodynamical properties and transport properties (thermal and electric conductivity) at extreme density, pressure, and temperature are thus of high interest.

Spectrally resolved X-ray Thomson scattering (XRTS) [4] provides accurate measurements of electron density and temperature in isochorically heated [5] and compressed matter via the shape of the plasmon resonance [6, 7] and the Compton feature [8]. In the Compton scattering regime, at large scattering angle, the plasma response is essentially uncorrelated, and the Compton profile reflects the single-particle distribution function which is fully characterized by electron density  $n_e$  and temperature  $T$ . Inferring these parameters by fitting the Compton profile calculated from first principles is hence model independent. Moreover, the electron temperature is constrained by the amount of elastic (Rayleigh) scattering. Finally, the average ionization per ion and hence the mass density is measured by observing Compton scattering from bound electrons visible at large energy shifts,

where free-free scattering is suppressed.

In this Letter, we present a novel method to directly infer information about the EoS of strongly compressed matter using XRTS. A beryllium sample is symmetrically compressed by two counter-propagating shock waves of equal strength producing densities of 3 and 6 times the solid density before and after the shock collision, respectively. In this Fermi degenerate plasma, the width of the Compton scatter profile provides a measure of the electron density  $n_e$  and is only weakly sensitive to the temperature. Thus measuring the first and second mass compression ratio we obtain sufficient information to infer  $\gamma$  at both instants. We solve the Rankine-Hugoniot equations for colliding shocks that govern the pressure- and density jump across the shock-front discontinuity and which contain  $\gamma$  as a parameter. Our results show that  $\gamma$  assumes relatively high values of 1.9(+0.7/-0.3) in the high compression regime, in agreement with a simple scaling model for  $\gamma$  [9] that is implemented e.g. in the SESAME EoS tables [10]. Within the error bars, this high compression value is consistent with the ideal gas limit  $\gamma = 5/3$ .

The experiment has been carried out at the Omega Laser at Laboratory for Laser Energetics, University of Rochester. Beryllium foils of 250  $\mu\text{m}$  thickness are symmetrically compressed by interaction with high energy laser pulses. A photograph of the target is shown in Fig. 1 (a), Fig. 1 (b) shows the setup. The Be foil is radiated from both sides by a total of twelve laser beams operating at 351 nm wavelength ( $3\omega$ ). Each beam delivers up to 480 J in a 1 ns long flat-top pulse onto a common focal spot of 800  $\mu\text{m}$  in diameter. Use of continuous phase plates yields a homogenous intensity profile across the focal spot. The pulses are staggered in time producing a constant intensity of  $2.0 \times 10^{14} \text{ W/cm}^2$  for 3 ns as shown in Fig. 1 (c) together with the resulting mass density evolution as simulated by the 1D radiation-hydrodynamics code HELIOS [11], applying the PROPACEOS EoS model.

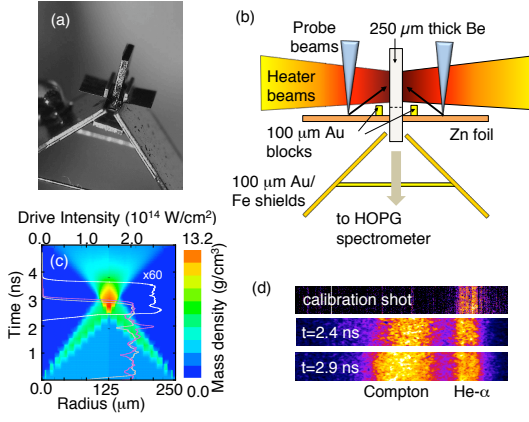


FIG. 1. (Color online) (a) Photograph of the target (b) Experimental setup (c) Rad-hydro simulation of the mass density evolution. Drive beam intensity profiles for each side (grey and purple) and x-ray probe pulse (white) are overlaid. (d) Raw x-ray scattering data. Top to bottom: Calibration shot, measuring the Zn He- $\alpha$  doublet; scattering before and after shock collision showing elastic and Compton scattering; increased Compton width is observed after after shock collision.

Simulations indicate that the shock waves collide in the target's center after 2.8 ns. Density and temperature conditions are homogeneous over spatial extensions of 25  $\mu\text{m}$  in the horizontal direction.

The plasma conditions are probed with x-ray Compton scattering [4] by laser produced Zn He- $\alpha$  radiation (photon energies of  $E_0 = 8.95 \text{ keV}$  and  $8.99 \text{ keV}$  for Zn He- $\alpha_1$  and He- $\alpha_2$ , respectively) and  $140^\circ \pm 10^\circ$  scattering angle. In the single-compressed matter, electron density of  $n_e = 8.6 \times 10^{23} \text{ cm}^{-3}$  is observed, rising to  $1.8 \times 10^{24} \text{ cm}^{-3}$  at shock-collision. High energy lasers produce the Zn He- $\alpha$  radiation. Pulses of 480 J energy and 1.0 ns duration are focused onto a Zn foil (200  $\mu\text{m}$  diameter focus), yielding intensities of  $\approx 1.5 \times 10^{16} \text{ W/cm}^2$ . The x-ray probe beams start 2.5 ns after the heater beams. At  $\theta = 140^\circ \pm 10^\circ$  scattering angle, the resulting  $k$ -vector is  $k = 2E_0 \sin(\theta/2)/\hbar c = (8.4 \pm 0.2) \text{ \AA}^{-1}$ . In Fig. 2, we show x-ray scattering spectra from compressed targets at 2.4 ns and 2.9 ns after the drive beam-target interaction, i.e. before and after shock collision, respectively. These X-ray spectra are measured by dispersing the scattered radiation in a large graphite crystal (highly-oriented pyrolytic graphite) onto an x-ray framing camera with 0.18 ns temporal resolution. A 100  $\mu\text{m}$  thick gold shield blocks the direct view of the spectrometer crystal to the intense x-ray probe source.

We observe elastic Rayleigh scattering from Zn He- $\alpha$  radiation at 8.95 keV and 8.99 keV along with a smaller contribution from Zn K- $\alpha$  radiation at 8640 eV. From the integrated Rayleigh feature we determine the plasma temperature using the high  $k$  limit (Debye-Hueckel model) for the ion-ion structure factor and the screening cloud

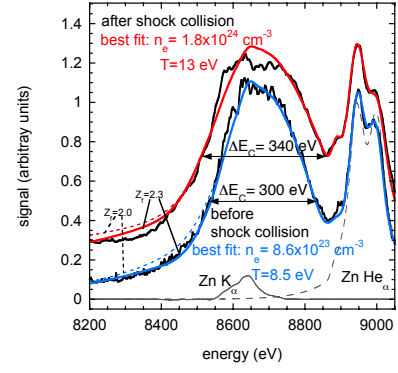


FIG. 2. (Color online) XRTS spectra before ( $t = 2.4 \text{ ns}$ ) and after ( $t = 2.9 \text{ ns}$ ) shock collision (+0.2 offset). XRTS simulations for the best-fit values for electron density  $n_e = 8.6 \times 10^{23} \text{ cm}^{-3}$  and temperature  $T = 9 \text{ eV}$  (blue) and  $n_e = 1.8 \times 10^{24} \text{ cm}^{-3}$ ,  $T = 13 \text{ eV}$  (red).  $Z_f = 2.3$  in both calculations, thin dashed lines:  $Z_f = 2.0$ . Zn He- $\alpha$  spectrum (black dashed) and the Zn K- $\alpha$  line (solid grey).

[12]. We find  $T = (10 \pm 2) \text{ eV}$  before shock collision and  $T = (15 \pm 2) \text{ eV}$  after shock collision. Results of this analysis are shown in the supplemental material [13].

Compton scattering from bound and free electrons is measured at a Compton shift of  $E_C = \hbar^2 k^2 / 2m_e \simeq 270 \text{ eV}$ . The width of the Compton peak substantially increases upon shock-collision from  $\Delta E_C = 300 \text{ eV}$  to  $\Delta E_C = 340 \text{ eV}$ . The Compton width depends on  $\sqrt{E_F} \propto n_e^{1/3}$  in this partly Fermi degenerate regime, where  $k_B T / E_F \simeq 0.3$ ,  $E_F = \hbar^2 (3\pi^2 n_e)^{2/3} / 2m_e = 31 \text{ eV}$  (52 eV) is the electron Fermi energy before (after) shock collision.

By comparing our experimental scattering spectra to calculations for the dynamical structure factor [4], we infer  $n_e$  and  $T$ . The data indicate that we are in the non-collective (Compton scattering) regime with scattering parameter  $\alpha = 1/k\lambda_s = 0.15$  ( $\lambda_s$  is the plasma screening length). In this regime, two-body correlations are negligible, the structure factor is only a function of  $n_e$  and  $T$  without any model dependence. Figure 3 shows contour lines for the mean square variance between fit curves and scattering data as function of  $n_e$  and  $T$ . From this analysis we obtain  $n_e = (8.6 \pm 0.7) \times 10^{23} \text{ cm}^{-3}$  and  $T = (9 \pm 2) \text{ eV}$  before shock collision and  $n_e = (1.8 \pm 0.2) \times 10^{24} \text{ cm}^{-3}$  and  $T = (12 \pm 3) \text{ eV}$  after shock collision, consistent with the temperature measurements using the Rayleigh peak.

Compton scattering from K-shell electrons contributes at photon energies below 8890 eV, corresponding to the K-shell ionization potential of  $\sim 110 \text{ eV}$  in the dense plasma, where continuum lowering of  $\sim 60 \text{ eV}$  is taken into account via the Stewart-Pyatt model [14]. The amount of bound-free scattering depends on the average ionization. We obtain good agreement with the data assuming  $Z_f = 2.3$ , consistent with earlier XRTS measurements of isochorically heated and shock-compressed Be [5, 15]. For single shock conditions similar to ours, Lee et al. [8] report  $Z_f = 2.0$ . However, calculations

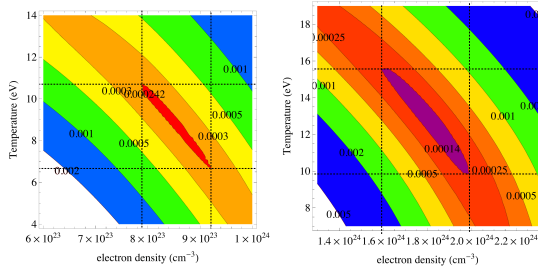


FIG. 3. (Color online) Contour lines for the mean square variance between fit curves and scattering data as function of  $n_e$  and  $T$ . The innermost contours define the error bars on  $n_e$  and  $T$ . (a) before shock collision, (b) after shock collision.

for  $Z_f = 2.0$  (thin dashed lines in Fig. 2) overpredict the bound-free contribution. Even at increased electron density during shock collision, ionization potential lowering is below 10 eV with respect to the single shocked state as estimated through the Stewart-Pyatt model. Hence, changes in  $Z_f$  between single and double shocked states are expected to be below the experimental resolution.

Correspondingly, the mass density rises from  $\rho_1 = (5.6 \pm 0.7) \text{ g/cm}^3$  to  $\rho_2 = (11.7 \pm 1.9) \text{ g/cm}^3$ . The uncertainties in  $\rho$  are the sum of uncertainties resulting from the  $n_e$  fitting procedure (see Fig. 3) and 5% uncertainty in  $Z_f$ . The compression increases from  $\rho_1/\rho_0 = 3.0$  to  $\rho_2/\rho_0 = 6.3$ , with respect to the solid mass density  $\rho_0 = 1.85 \text{ g/cm}^3$ . Here and in the following, we denote conditions in the uncompressed material by the index 0, the single shock compressed matter by index 1, and the region of shock overlap by index 2.

We apply the Rankine-Hugoniot equations [16] to determine the adiabatic index  $\gamma$ . The Rankine-Hugoniot equations follow from the conservation of total mass, energy, and momentum. They relate the particle velocities  $u_0, u_1$ , pressures  $p_0, p_1$  and mass densities  $\rho_0, \rho_1$  in the uncompressed and in the compressed region, respectively. One finds for the energy jump across the shock front

$$\varepsilon_0 - \varepsilon_1 = (p_0 + p_1) (1/\rho_1 - 1/\rho_0)/2. \quad (1)$$

These relations hold for each individual shock as well as for the two shock fronts that evolve after the shock collision between the single and the doubly shocked material and which travel in opposite directions away from each other. The adiabatic index  $\gamma$  is introduced to eliminate the internal energy  $\varepsilon = p/(\gamma - 1)\rho$ . Accounting for different values of  $\gamma$  before and after compression, one derives for the compression ratio

$$\frac{\rho_1}{\rho_0} = \left[ 1 + \frac{p_1}{p_0} \frac{\gamma_1 + 1}{\gamma_1 - 1} \right] / \left[ \frac{p_1}{p_0} + \frac{\gamma_0 + 1}{\gamma_0 - 1} \right] \quad (2)$$

Preheat due to fast electrons generated on the target's surface is negligible: At our drive laser intensities, hot electrons with  $\langle E_{\text{hot}} \rangle = 3 \text{ keV}$  average energy, estimated by resonance absorption [17], penetrate only the first

$9 \mu\text{m}$  [18]. Correspondingly,  $p_0 \ll p_1$ , we are in the strong shock limit, where one recovers the familiar result

$$\lim_{p_1/p_0 \rightarrow \infty} \frac{\rho_1}{\rho_0} = \frac{\gamma_1 + 1}{\gamma_1 - 1}. \quad (3)$$

Note that the strong shock compression depends only on  $\gamma_1$ , i.e. the conditions in the compressed region. For a perfect monoatomic gas with  $\gamma = 5/3$ , one obtains  $\lim_{p_1/p_0 \rightarrow \infty} \rho_1/\rho_0 = 4$ . The residual level of density fluctuations due to shock induced turbulence after the first shock is estimated following Ref. [19] as  $\sqrt{\langle \delta \rho \delta \rho \rangle} / \rho_1 \simeq 1\%$ , i.e. within the experimental error bars. Undercompression due to turbulence is therefore neglected.

The jump in particle velocities can be expressed as

$$(u_i - u_j)^2 = (1 - \rho_i/\rho_j) (p_j/p_i - 1) p_i/\rho_i. \quad (4)$$

In the case of two colliding strong shocks, symmetry of the problem with respect to the contact surface between the two shock waves at the moment of collision completely determines the final compression [20]. In particular, the material at the contact surface is at rest,  $u_2 = 0$ . Furthermore, the material velocity in the unshocked material  $u_0$  is negligible compared to  $u_1$ , the velocity in the first, strongly shocked material region. From the two forms of eq. 4 corresponding to  $|u_2 - u_1| = u_1$  and  $u_1 = |u_1 - u_0|$  we find a quadratic equation for the compression ratio  $\rho_2/\rho_1$

$$\frac{2 \frac{\rho_2}{\rho_1} \gamma_1 \frac{\gamma_2 - 1}{\gamma_1 - 1} - 2 \gamma_2 \frac{\frac{\rho_2}{\rho_1} - 1}{\frac{\rho_2}{\rho_1}}}{\frac{\rho_2}{\rho_1} (1 - \gamma_2) + \gamma_2 + 1} = \frac{\rho_1}{\rho_0} - 1. \quad (5)$$

For a system with constant adiabatic index  $\gamma_2 = \gamma_1 = \gamma_0$ , one recovers the result  $\frac{\rho_2}{\rho_1} = [2 + (\gamma + 1)(\frac{\rho_1}{\rho_0} - 1)] / [2 + (\gamma - 1)(\frac{\rho_1}{\rho_0} - 1)]$  for the second compression [20]. For the ideal gas  $\frac{\rho_2}{\rho_1} = 2.5$ .

Using our measured mass density values, we find the adiabatic indices  $\gamma_1, \gamma_2$  by inverting relations (3) and (5),

$$\gamma_1 = (\rho_1 + \rho_0) / (\rho_1 - \rho_0) \quad \gamma_2 = \rho_2 / (\rho_2 - \rho_1) \quad (6)$$

For the single compressed Be before shock collision we obtain  $\gamma_1 = 2.0 \pm 0.2$  at  $\rho_1 = (5.6 \pm 0.7) \text{ g/cm}^3$  and  $\gamma_2 = 1.9^{+0.7}_{-0.4}$  at  $\rho_2 = (11.7 \pm 1.9) \text{ g/cm}^3$  for the material after the collision.

Figure 4 shows our data (red points) for the adiabatic index reaching high densities of  $\sim 12 \text{ g/cm}^3$ . Vertical error bars on  $\gamma_2$  result from the dependence on  $\rho_1$  and  $\rho_2$ . The black diamond shape point is inferred from the single shock compression data from Lee et al. [8] in excellent agreement with our measurement before shock collision.

For comparison, we also show measurements of the sound speed gamma  $\gamma_S$  from explosion experiments (squares and triangles) inferred through shock-wave radiography by Neal [21]. The two data sets correspond

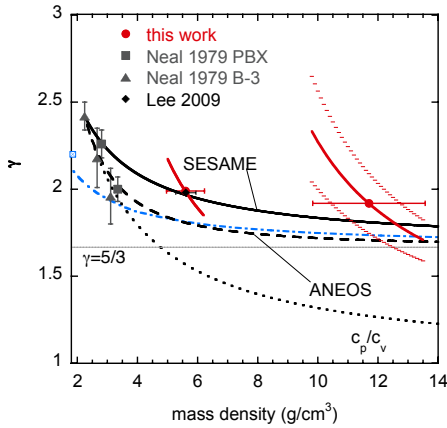


FIG. 4. (Color online) Adiabatic index  $\gamma$  for compressed Be measured by XRTS (Red points). Vertical error bars on the high compression point result from the dependence of  $\gamma_2$  on  $\rho_1$  and  $\rho_2$ . Black diamond: compression data by Lee et al. Squares and triangles at low compression measurements of  $\gamma_S$  by Neal et. al. Analytical expressions for  $\gamma_S$  used in SESAME EoS (solid) and in the ANEOS model (dashed) and linear model for  $c_p/c_v$  (dotted). Dash-dotted (blue): DFT EoS simulation for  $\gamma_S$ , blue square: solid Be quoted by Rudin et al.

to different explosives used to generate the shock wave. Shock pressures in the 30 GPa range are reported, where Be is in the bcc phase. The dashed blue curve is a density-functional theory (DFT) simulation for  $\gamma_S$  [22] in hcp Be, the blue square is the experimental point for  $\gamma_S$  for solid hcp Be as quoted by the same authors. The black solid curve is an analytic expression for  $\gamma_S$  that is implemented in the generator of the SESAME EoS tables [10],  $\gamma_S(\rho) = \gamma_S(\rho_0)\rho_0/\rho + 5(1 - \rho_0/\rho)/3$  [9], the black dashed curves are taken from the ANEOS model [23] which assumes quadratic scaling in  $\rho/\rho_0$  instead of the linear behavior implemented in SESAME. The reference point  $(\rho_0, \gamma_0)$  is fixed at the point for lowest compression reported by Neal. These theoretical models converge to the high density (Fermi degenerate) limit  $\gamma(\rho \gg \rho_0) = 1.67$ . Also our data seem to go to that limit, although more slowly. Finally, the dotted (black) curve is a linear scaling model for the ratio of heat capacities  $c_p/c_v = 1 + (c_p/c_v)_0 - 1)\rho_0/\rho$ ; at high densities  $c_p/c_v = 1$  [24].

Our results clearly demonstrate that the adiabatic index is significantly different from the heat capacity ratio. The SESAME model for  $\gamma_S$  with respect to the lowest compression point by Neal lies within the error bars for both single and double shocked Be but tends to slightly underestimate  $\gamma$ . The ANEOS model and the DFT simulation for  $\gamma_S$  are not consistent with our shock-gamma measurements at single compression. At high compression, all models converge to the ideal gas 5/3 and are consistent with our data within the error bars. On the other hand, data from Neal at increased compression agree only with the ANEOS model and also with the  $c_p/c_v$  scaling.

We found  $\gamma = 1 + p/\rho\varepsilon$  being substantially higher than 5/3 at single compression, which means in turn that  $p/\rho\varepsilon$  exceeds the ideal gas value 2/3. This is in agreement with quantum mechanical EoS calculations for dense, partly degenerate plasmas [25]. Exchange contributions are the dominant terms, leading to a decrease in pressure and in internal energy, the latter being much more pronounced (up to 80% with respect to the ideal gas value vs. 10% reduction in pressure). The net effect is an increase in the adiabatic index  $\gamma = 1 + p/\rho\varepsilon$ . Also at double compression, the relatively high value for  $\gamma_2 = 1.9$  would indicate a reduced single-shock compressibility (c.f. eq. (3)) by 20% with respect to  $\gamma = 5/3$ . However,  $\gamma = 5/3$  is still consistent with our data within the error bars and a decisive statement cannot be made.

In conclusion, we have measured the mass density increase in Be upon shock compression by two counter-propagating shock waves before and after the shock collision. From the Hugoniot relations we inferred  $\gamma$  at two mass densities. Our results agree with a linear model used in the SESAME EoS. They show the departure from the ideal gas behavior  $\gamma = c_p/c_v$  at single shock compression, consistent with a reduction in internal energy due to the exchange interaction in partly degenerate plasmas. The presented novel technique has great potential for applications in material research, inertial confinement fusion and laboratory astrophysics. To this end, we need to improve the resolution in the mass density measurement by reducing the Zn K- $\alpha$  emission and by taking an average over multiple shots to increase the signal to noise ratio. We also plan to perform high precision measurements using x-ray free electron laser radiation where we take advantage of the larger photon number at smaller bandwidth to improve signal to noise and increase the separation between inelastic and elastic scattering components, allowing for a more detailed and accurate density and temperature measurement.

This work was performed under the auspices of the U.S. Department of Energy by Lawrence Livermore National Laboratory under Contract DE-AC52-07NA27344 and supported by LDRD grant 10-ER-050. C.F. acknowledges support by the Alexander von Humboldt-Foundation. We thank A. Pak and L. Divol for helpful discussions.

- 
- [1] J. D. Lindl, P. Amendt, R. L. Berger, S. G. Glendinning, S. H. Glenzer, S. W. Haan, R. L. Kauffman, O. L. Landen, and L. J. Suter, *Phys. Plasmas* **11**, 339 (2004).
  - [2] R. P. Drake, *High Energy Density Physics* (Springer, 2006).
  - [3] D. C. Wilson, *Phys. Plasma* **42**, 1952 (1998).
  - [4] S. H. Glenzer and R. Redmer, *Rev. Mod. Phys.* **81**, 1625 (2009).
  - [5] S. H. Glenzer, O. L. Landen, P. Neumayer, R. W. Lee, K. Widmann, S. W. Pollaine, R. J. Wallace, G. Gregori, A. Höll, T. Bornath, R. Thiele, V. Schwarz, W.-D.

- Kraeft, and R. Redmer, Phys. Rev. Lett. **98**, 065002 (2007).
- [6] A. L. Kritcher, P. Neumayer, J. Castor, T. Döppner, R. W. Falcone, O. L. Landen, H. J. Lee, R. W. Lee, E. C. Morse, A. Ng, S. Pollaine, D. Price, and S. H. Glenzer, Science **322**, 69 (2008).
- [7] P. Neumayer, C. Fortmann, T. Döppner, P. F. Davis, R. W. Falcone, A. L. Kritcher, O. L. Landen, H. J. Lee, R. W. Lee, C. Niemann, S. Le Pape, and S. H. Glenzer, Phys. Rev. Lett. **105**, 075003 (2010).
- [8] H. J. Lee, P. Neumayer, J. Castor, T. Döppner, R. W. Falcone, C. Fortmann, B. A. Hammel, A. L. Kritcher, O. L. Landen, R. W. Lee, D. D. Meyerhofer, D. H. Munro, R. Redmer, S. P. Regan, S. Weber, and S. H. Glenzer, Phys. Rev. Lett. **102**, 115001 (2009).
- [9] L. Davison, *Fundamentals of Shock Wave Propagation in Solids* (Springer, Heidelberg, 2008).
- [10] S. Lyon and J. Johnson, *Los Alamos National Laboratory, Los Alamos, NM, LA-UR-92-3407*, Database Technical report LA-UR-92-3407 (Los Alamos National Laboratory, 1992).
- [11] J. MacFarlane, I. Golovkin, and P. Woodruff, J. Quant. Spectrosc. Radiat. Transfer **99**, 381 (2006).
- [12] D. Kremp, M. Schlanges, and W.-D. Kraeft, *Quantum Statistics of Nonideal Plasmas*, Atomical, Optical and Plasma Physics (Springer, Heidelberg, Berlin, New York, 2005).
- [13] “See supplemental material at [url will be inserted by publisher] for determination of the plasma temperature  $T$  from the elastic scattering component.”.
- [14] J. C. Stewart and K. D. Pyatt Jr., Astrophys. J. **144**, 1203 (1966).
- [15] A. Kritcher, T. Döppner, C. Fortmann, O. Landen, R. Wallace, and S. Glenzer, High Energy Dens. Phys. **7**, 271 (2011).
- [16] Y. Zel’Dovich and Y. Raizer, *Physics of shock waves and high-temperature hydrodynamic phenomena*, edited by W. D. Hayes and R. F. Probstein (Dover Pubns, Mineola, New York, 2002).
- [17] W. Kruer, *Handbook of Plasma Physics*, edited by A. Rubenchik and S. Witkowski, Vol. 3 (Westview Pr, Amsterdam, 2003).
- [18] S. Atzeni, Phys. Plasmas **6**, 3316 (1999).
- [19] G. Hazak, A. L. Velikovich, J. H. Gardner, and J. P. Dahlburg, Phys. Plasmas **5**, 4357 (1998).
- [20] H. Motz, *The Physics of Laser Fusion* (Academic Press, London, 1979).
- [21] T. Neal, in *High-Pressure Science and Technology*, AIRAP Conference Proceedings, Vol. 1 and 2, edited by K. D. Timmerhaus and M. S. Barber (Plenum Press, New York, 1979).
- [22] S. P. Rudin, M. D. Jones, and J. D. Johnson, in *Proceedings of the Joint 20th AIRAPT and 43rd EHPRG International Conference on High Pressure Science and Technology* (2005) p. O058.
- [23] S. Thompson and H.S. Lawson, *Improvements in the CHART D Radiation- Hydrodynamic Code IH: Revised Analytic Equations of State*, Tech. Rep. SC-RR-710714 (Sandia National Laboratories, Albuquerque, NM, 1972).
- [24] G. P. Horedt, *Polytropes - Applications in Astrophysics and Related Fields* (Kluwer Academic, Dordrecht, 2004).
- [25] J. Vorberger, M. Schlanges, and Kraeft, W.D., Phys. Rev. E **69**, 046407 (2004).